Methane Hydrates: Nucleation in Microporous Materials

Eduardo Andres-Garcia, Alla Dikhtiarenko, Francois Fauth, Joaquin Silvestre-Albero, Enrique V. Ramos-Fernández, Jorge Gascon, Avelino Corma, Freek Kapteijn

PII: S1385-8947(18)32450-1
DOI: https://doi.org/10.1016/j.cej.2018.11.216
Reference: CEJ 20518

To appear in: *Chemical Engineering Journal*

Received Date: 10 October 2018
Revised Date: 26 November 2018
Accepted Date: 28 November 2018

Please cite this article as: E. Andres-Garcia, A. Dikhtiarenko, F. Fauth, J. Silvestre-Albero, E.V. Ramos-Fernández, J. Gascon, A. Corma, F. Kapteijn, Methane Hydrates: Nucleation in Microporous Materials, *Chemical Engineering Journal* (2018), doi: https://doi.org/10.1016/j.cej.2018.11.216

Methane Hydrates: Nucleation in Microporous Materials

Eduardo Andres-Garcia[1]*, Alla Dikhtiarenko[2], Francois Fauth[3], Joaquin Silvestre-Albero[4], Enrique V. Ramos-Fernández[4], Jorge Gascon[2], Avelino Corma[5] and Freek Kapteijn[1]*

[1]Catalysis Engineering , ChemE, TU Delft, Van der Maasweg 9, 2629HZ, Delft, The Netherlands

[2]King Abdullah University of Science and Technology, KAUST Catalysis Center, Advanced Catalytic Materials. Thuwal 23955-6900, Saudi Arabia

[3]ALBA Synchrotron, Cerdanyola del Vallès, 08290 Barcelona, Spain

[4]Laboratorio de Materiales Avanzados, Universidad de Alicante, San Vicente del Raspeig, Spain

[5]Instituto Universitario de Tecnología Química CSIC-UPV, Valencia, Spain

*f.kapteijn@tudelft.nl, e.andresgarcia-1@tudelft.nl, tel: +31 (0) 15-2783516

Clathrates are well-known compounds whose low thermal stability makes them extremely rare and appreciated. Although their formation mechanism is still surrounded by many uncertainties, these ice-like structures have the potential to be an alternative for transport and storage of different gases, especially methane. For the formation of methane clathrates extreme pressure conditions and a narrow temperature window are needed. Microporous materials have been proposed to provide nucleation sites that, theoretically, promote clathrate formation at milder conditions. While activated carbons and Metal-Organic Frameworks (MOFs) have already been studied, very little is known about the role of zeolites in this field. In this work, we study the formation of methane clathrates in the presence of RHO zeolite. Experimental results based on adsorption and operando synchrotron X-Ray diffraction demonstrate the formation of clathrates at the surface of the zeolite crystals and reveal mechanistic aspects of this formation at mild conditions.

Keywords: Adsorption; Clathrate; Zeolite; RHO; Nucleation; Methane Hydrate

1. Introduction

Gas clathrates (or gas hydrates) are crystalline ice-like nonstoichiometric compounds based on water molecules linked by hydrogen bonds hosting a gas molecule (with van der Waals bonds between it and the clathrate structure). The water molecules of the structure form a regular cage through hydrogen bonds, leading to various crystal lattices. The cages differ in their shape, size and capacity, but they always maintain a proportion in a range of 5.66 and 5.75 H_2O molecules per guest molecule, depending on the final clathrate structure. These cages are classified in three main final structures, known as I, II and H (Figure 1), where capacity and stability are the most defining parameters [1]. Structure I (denoted as *sI*) and Structure II (*sII*) were already discovered and identified in the 1950s [2-5], *sI* hydrates host small gas molecules such as H_2, CO_2 or CH_4; even with a low occupancy factor, they sometimes allow more than one of the smallest molecules inside their cages (such as hydrogen) [6]. This structure is the first to appear, but it is also the most instable. By contrast, *sII* is the largest structure and the most stable. Some promoters can induce the formation of this structure even with the smallest host gases. In this case, the biggest molecule will act as a template of the cage, reducing the potential capacity but increasing stability. Tetrahydropyran (THP) and tetrahydrofuran (THF) are two of the reported promoters of *sII* for methane hydrates, as all interactions (guest-guest, guest-host and especially host-host) affect the cages expansion [7]. It is remarkable that both THP and THF promote the formation of CH_4 clathrates, theoretically allowing gas separation processes due to differences in the final structure (*sII* against *sI* for CO_2 or N_2) [8, 9]. Structure H – for its hexagonal shape – is able to host bigger molecules than the previous ones, including hydrocarbons [10].

By examining the structures I, II and H, seven cage types were discovered, which comprise 95% of all the cages formed in clathrates. This set includes the 5^{12} cage, and $5^{12}6^n$ - $4^15^{10}6^n$ (in both cases, n ranges between 2 and 4), including the irregular dodecahedron of $4^35^66^3$ and the icosahedron of $5^{12}6^8$ [6, 11].

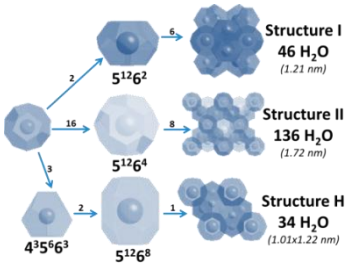

Figure 1. Clathrate´s structures: cages, water units and (reproduced from reference 12 with permission from ELSEVIER) [12].

The conditions of clathrate formation are extremely specific: temperatures must be close to 273 K and pressures have to rise above 35 bar, thus limiting its natural appearance to under continental shelf margins and beneath permafrost [13]. However, even with their specific range of appearance, natural methane hydrates are believed to be the largest source of hydrocarbons on Earth [14]. They can be found all over the world and comprise vast storages of methane. Methane reserves in Japan are estimated to be able to supply the country with energy for the coming 100 years. Thus, mimicking nature, the use of clathrates for methane storage can be envisaged as an interesting alternative to conventional processes (e.g. compressed or liquefied gas), that is gaining importance due to the complete reversibility of the process, in addition to safety and economical concerns. Clathrates can be an alternative as energy source and storage material, once its formation mechanism is understood and controlled [15, 16].

As there is a necessity of solid-liquid-gas interphase for bulk clathrate formation, the presence of nanoporous spaces is advantageous, by increasing the contact surface and allowing hydrates to grow under milder conditions and faster kinetics. The use of these materials as hosts for the formation of clathrates has been studied in the last few years [14, 17-19]. It has been tentatively proposed that these materials act as a template, a nucleation centre for the formation of clathrates; however, the mechanism is not completely understood [10, 20]. Some publications have reported that gas supersaturation results in spontaneous formation of clathrates [21, 22]. However, other authors have attributed it to memory effects and residual structures – molten hydrates persist in liquid after dissociation providing nucleation sites – and external impurities may promote the appearance of these

frameworks [23, 24]. Hydrate formation generally begins at a vapour/liquid interface rather than in the bulk liquid, or, in the case of template presence, at its surface. Once pressure and temperature are in the suitable range, gas molecules dissolve in water and form a '*blob*' – long-lived aggregates of guest molecules separated by water molecules – as precursor of the clathrate [25, 26]. An amorphous hydrate makes its appearance with two possible ends: decomposing or becoming stable. If stability is the final goal and the agglomerate reaches a critical value, small cages (5^{12}) initiate the final structure, while more water molecules join the framework to develop bigger cages and more stable clathrates [16, 20, 27].

As mentioned above, the promoting effect of activated carbons and MOFs in clathrate formation has been confirmed [14, 17], thus a logical question manifests itself: would zeolites also provide similarly nucleation sites under milder conditions? Some preliminary results have been already published, in an attempt to reveal new information about methane clathrates formation mechanism [28]. Zeolites are crystalline aluminosilicates based on tetrahedral structural units (SiO_4 and AlO_4) [29, 30]. Their high thermal and chemical stability make these materials ideal for use in many different applications [31]. The RHO topology, used in this study, is composed of a body-centered-cubic arrangement of truncated cubooctahedra or α-cages linked via double 8-ring building units (thus, it is classified as a small-pore zeolite), giving rise to two interpenetrating but not interconnected pore systems [32]. The pore diameter of this zeolite is 0.36 nm and its Si/Al ratio is 4.1 (promoting a hydrophilic behaviour). It contains sodium-cesium cations in its framework (Na, Cs-RHO). Despite the strength of the Si-O bond (one of the strongest in nature); some zeolites can also display flexibility in response to external stimuli. RHO exhibits atypical framework flexibility. It can adopt either a centric (*C*-form, *Im*-3*m*) (Figure 2.a) or an acentric (*A*-form, *I*-43*m*) symmetry (Figure 2.b), expressed as a distortion of the 8R structure from circular (0.36 nm) to elliptical (0.29 nm) geometry and a contraction of α cages from the initial cubic to tetrahedral driven by a relocation of cations from D8R to S6R sites [32, 33]. This structure disturbance is the effect of hydration (from cubic *I*-43*m* to *Im*-3*m*) [34, 35]. This special property presents RHO as a promising candidate in gas separa-

tion processes [36].

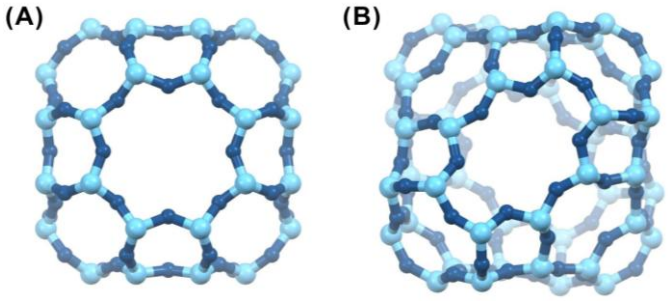

Figure 2. Flexibility of the RHO zeolite framework leading to two network configurations: (*a*) centric RHO (hydrated) form crystallized in cubic *Im*-3*m* space group and (*b*) acentric RHO (dehydrated) form having cubic *I*-43*m* configuration.

In this work, by applying gas adsorption measurements and operando X-Ray diffraction, we demonstrate that the surface of RHO zeolite can act as nucleation site for the formation of methane hydrates at mild conditions.

2. Materials and method

2.1. Sample preparation

Na,Cs - RHO was selected for this study; the zeolite was synthesized following the protocol from Pera-Titus et al.31 and provided by ITQ (Instituto de Tecnología Química) [32, 37]. The pore diameter of this 8-membered-ring zeolite (0.36 nm) makes it the most suitable to work with methane – with a kinetic diameter of 0.38 nm. The proximity of sizes will promote an adsorption regulated by temperature, pressure and hydration conditions: three parameters to control and understand the whole nucleation process. In order to standardize the process, the sample was calcined at 873 K before every experiment. The sample was firstly hydrated through vapour phase saturation with miliQ water (0 - 5 mol% THF) at room temperature, tetrahydrofuran is added as a promoter for *sII* structure. For the last methane isotherms, hydration changed from vapour phase to liquid phase (in excess of pore volume), and the wet sample was frozen before the measurements [17].

2.2.Sample characterization

Scanning electron microscopy (SEM) and energy-dispersive X-ray spectroscopy (EDS) provide information about external morphology, chemical composition, and crystalline structure of the analysed sample. The instrument used was a JEOL JSM-6010LA microscope. Gas adsorption was measured by volumetric method. Low-pressure experiments (below 1 bar) were measured in a Micromeritics TriStar II 3020, to estimate the pore volume of the sample. Nitrogen (at 77 K) is the most commonly used gas for this purpose, but the pore diameter of RHO zeolite makes it unviable. Water isotherms, at 298 K, were the chosen alternative. High-pressure adsorption experiments (up to 40 bar) were conducted using a BELSORP-HP. The adsorption/desorption isotherms for CO_2 and CH_4 were obtained with an equilibration time from 600 to 60,000 seconds. Temperature ranged from 273 K to 323 K. In dry cases, the samples were outgassed overnight under vacuum conditions at 473 K.

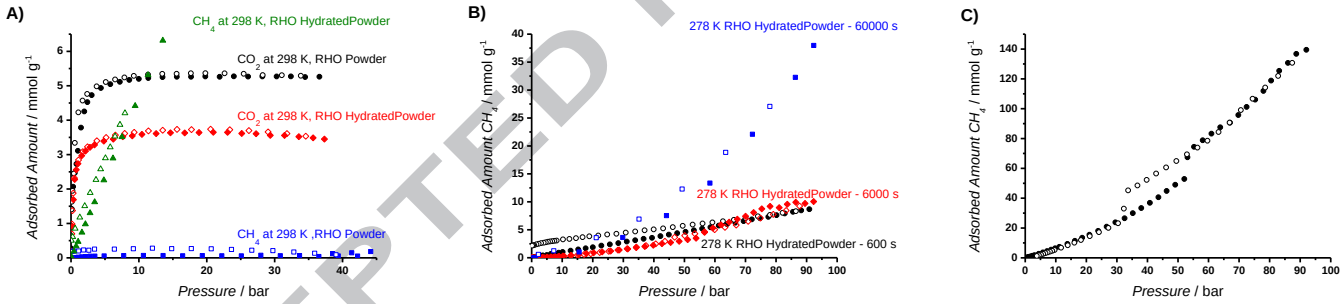

Figure 3. (*a*) CO_2 and CH_4 adsorption/desorption isotherms measured at 298 K for dry and hydrated (miliQ water) RHO zeolite powder, at equilibration time of 600 s. (*b*) CH_4 adsorption/desorption isotherms measured at 278 K over hydrated (5% THF miliQ water) RHO zeolite at different equilibration times: 600 (black, circle), 6,000 (red, diamond) and 60,000 s (blue, square) . (*c*) CH_4 adsorption/desorption isotherm measured at 275 K over hydrated (5% THF miliQ water) RHO zeolite at equilibration time of 60,000 s. Solid symbols correspond to the adsorption branch and open ones for desorption.

2.3.Operando PXRD measurements

In situ powder X-ray diffraction (PXRD) patterns of hydrated RHO zeolite were measured at ALBA synchrotron (Barcelona, Spain), using a wavelength λ = 0.5336 Å. Data was collected in the high-pressure end station of the MSPD beamline. For hydration experiments, 3 MPa of CH_4 was supplied

to the sample. The wet sample experiments were performed from 273 K to 243 K by stepwise changing the temperature (keeping the sample at the desired temperature for 30 min); the wet sample pressurised with methane was similarly recorded from 273 K to 233 K, and stepwise increasing to 275 K – the temperature at which clathrate melted and its structure decompose.

Phase quantitative analyses and Le Bail refinements have been done using MAUD software [38]. Crystal size and strain calculations were performed considering instrumental broadening parameters which have been determined measuring LaB_6 NIST 660b as a standard.

3. Results and Discussion

3.1.Sample characterization

The images obtained with scanning electron microscope reveal a homogeneous distribution of RHO zeolite particles, presenting spherical crystallites of ~1.5 μm (Figure A.1). A water isotherm (Figure A.2) was measured at 298 K to estimate the pore volume on RHO which estimated to be 0.23 cc(liq) g^{-1}. Adsorption starts at low pressure due to the hydrophilic behaviour of the zeolite. A small hysteresis loop is present at low pressure attributed to the hydration structural change.

Pure component high-pressure adsorption isotherms for carbon dioxide and methane are presented in Figures A.3 and A.4, respectively. Carbon dioxide values correlate with theoretical expectations. The methane uptake profiles cannot even be considered as isotherms because equilibrium is not achieved. The uptake values are negligible, only at higher temperatures activated diffusion results in some uptake. Also the large adsorption-desorption hysteresis evidences diffusion limitations, due to the similar size of the methane molecule and RHO pore diameter.

Hydration affects the pore diameter in RHO zeolite due to its flexible framework. In Figure 3, the hydration effect is studied for CO_2 and CH_4 adsorption (at 298 K). For carbon dioxide a decrease in capacity results because adsorbed water is occupying part of the pore volume (Figure 3.a). On the contrary, hydration allows methane to enter the framework due to the enlargement of the pores. This effect is also evidenced in Figure 3.a. However, the amount of methane adsorbed in the wet

sample does not seem compatible with the free pore volume of the zeolite [36, 39].

These results are a strong indication of the presence of methane hydrate (methane clathrate), especially considering the unusual conditions of the experiment (the complete isotherm can be found in appendix as Figure A.8). Reproducibility was the initial issue, but it was resolved by adjusting hydration (5 mol % THF miliQ water) and measurement conditions (278 K and 100 bar); Hydration was also modified, from vapour phase to liquid phase, adding water in excess to avoid limitations in clathrates formation. That wet sample was frozen before the experiments.[17] Figure 3 also demonstrates the impact of a fourth parameter that needs to be considered: the equilibration time. Clathrate formation kinetics are known to be slow [40, 41]; testing different equilibration times while recording the isotherms (from 600 s to 60,000 s) confirms this assumption and presents time as the key parameter to control this process (Figure 3.b). Setting a longer equilibration time for each isotherm point allows clathrate's growing; a suitable equilibration time is as important as temperature/pressure conditions, for clathrate formation. By comparing zeolite capacity with 'adsorbed' methane from the previous figures, it is clear that it is physically impossible to explain those large adsorption amounts. After confirming the absence of leaks or other technical problems, clathrate formation is the most rational explanation. In addition, the hysteresis shown in Figure 3c corresponds with reported hydrate formation in hydrated microporous materials [14, 17].

All methane uptake profiles (Figure 3.b-c) show a change in their slope around 3.5 mmol g^{-1}, which corresponds to the free pore volume in a hydrated sample: methane firstly saturates the hydrated zeolite (drying the material by displacing the water in it) and secondly gets accumulated around it, in hydrates cages. The pre-hydration of the micropores stabilizes the methane adsorption and promotes a better organization leading to hydrate formation [42]. Considering the diameter of those hydrate cages (1.20 nm against the 0.36 nm of the pore) excludes the possibility of clathrate formation inside the pores. Thus, the hydrated microporous material is presumably acting as nucleation site, promoting methane clathrate formation on the external crystal surface. The end of the adsorption branch, after the hysteresis, is probably the most interesting zone of the isotherm: clathrates are

still growing, but no further hysteresis is observed. This growth is pressure-dependent, methane interaction with the already formed hydrates is the key of this isotherm section.

3.2.Operando PXRD measurements

Temperature dependent PXRD patterns of hydrated zeolite were recorded at 273 K and at stepwise decreased temperatures down to 243 K and increasing it back up to 273 K (Figures 4.a-b). Under these conditions, the hydrated zeolite sample reveals the presence of both centric (*Im*-3*m*) and acentric (*I*-43*m*) phases corresponding to regular and distorted configurations of the RHO framework (Figure 4.a). As can be observed from the Figure 4.b, the formation of crystalline ice takes place at 243 K which is evidenced by typical reflections of the I_h hexagonal ice structure ($P6_3cm$) [43]. As soon as the temperature increases, the intensity of the ice-related diffraction lines starts to decrease and at 273 K the ice present in the system becomes amorphous (Figure 4.b). In order to evaluate the composition of the mixture at each temperature, quantitative phase analysis was performed. The results summarized in Figure 4.c suggest that at room temperature the hydrated zeolite sample contains 14 wt% of the acentric RHO phase. Notably, as soon as the temperature decreases and crystalline ice forms, the weight fraction of acentric RHO form increases up to 18 wt%. Moreover, the appearance of I_h ice is accompanied by an increase in the ratio between *C*-form (*Im*-3*m*) and A-form (*I*-43*m*). Two explanations can account for this phenomenon: (*i*) participation of semi-hydrated acentric RHO-form in the ice formation process, and (*ii*) the coexistence of *C*- and *A*-forms of RHO network as individual crystallite domains within the same zeolite grain. The quantitative phase analyses suggest that once the ice starts to grow as crystalline phase, the hydrated zeolite sample become dryer which is reflected on the *A*-RHO weight fraction rise.

Thus, the centric phase of RHO zeolite transforms into dehydrated acentric RHO form as an effect of the ice crystals formation, drawing water molecules towards the nucleation centres where the crystalline ice growth is taking place. Furthermore, the variation of unit cell parameters for each of crystalline phases present in the hydrated zeolite sample were evaluated over temperature range between 273 K and 243 K down, and back again up to 273 K. As can be observed from Figure 5.a, the

formation of I_h ice crystals is correlated with the structural changes of semi-hydrated acentric RHO-form and reflected on the disturbance of its unit cell parameters whereas no significant changes in corresponding values for the centric phase were noted. Furthermore, the ice formation process was evaluated by following the crystal size and macrostrain changes over the studied range of temperatures. As can be observed in Figure 5.b, the ice crystallization starts at 243 K and the crystals continue growing up to 273 K. Since the macrostrain parameter is inversely proportional to crystal size, an identical trend can be observed on the corresponding macrostrain curves for I_h ice crystallites revealing a continuous growth process. Excluding the epitaxial and structural intergrowth between ice and both forms of the RHO zeolite frameworks, and considering the large difference between pore volume for both forms of RHO zeolite and the sizes of the ice crystals formed in the system, it can be concluded that the growth of I_h ice crystals is taking place at the zeolite grain surface.

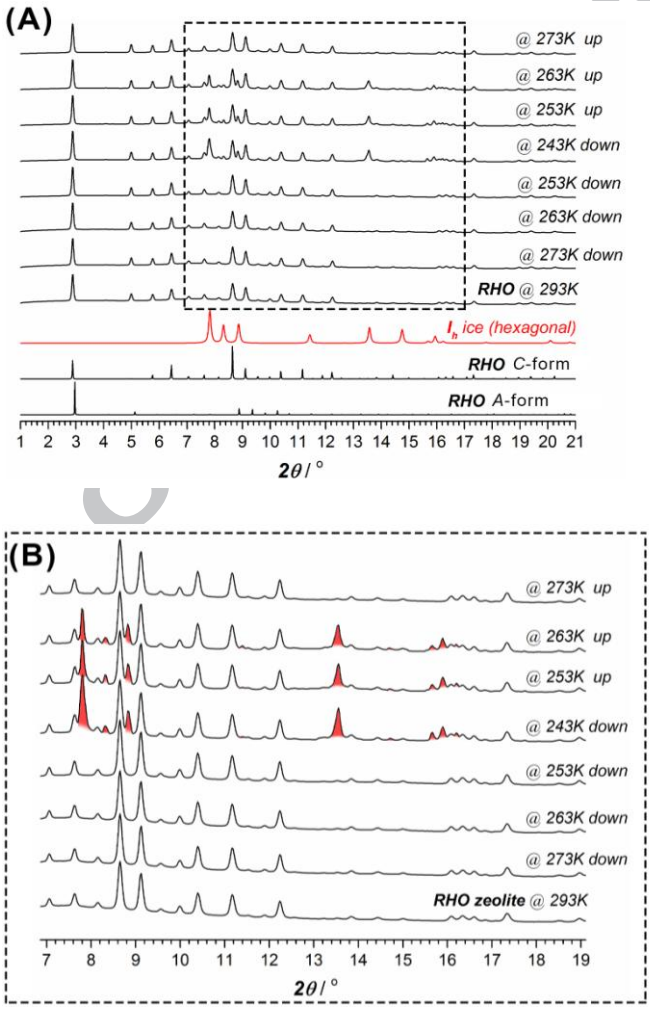

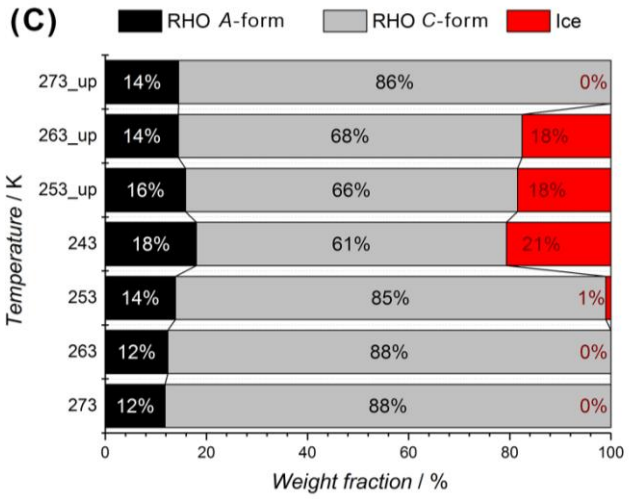

Figure 4. (*a*) Comparison of powder X-ray diffraction patterns of hydrated RHO zeolite at different temperatures, down from 273 K to 243 K and up again to 273 K, and expected diffraction patterns for centric (*Im*-3*m*) and acentric (*I*-43*m*) phases of RHO zeolite and I_h hexagonally packed ice structure ($P6_3cm$). (*b*) Inset shows the enlarged 2θ region where typical diffraction lines (highlighted in red) originated from the hexagonal ice structure (I_h) are visible. (*c*) The evolution of the weight fraction for centric, acentric phases of RHO zeolite and crystalline ice in the mixture over temperature range from 273 K to 243 K and up again to 273 K.

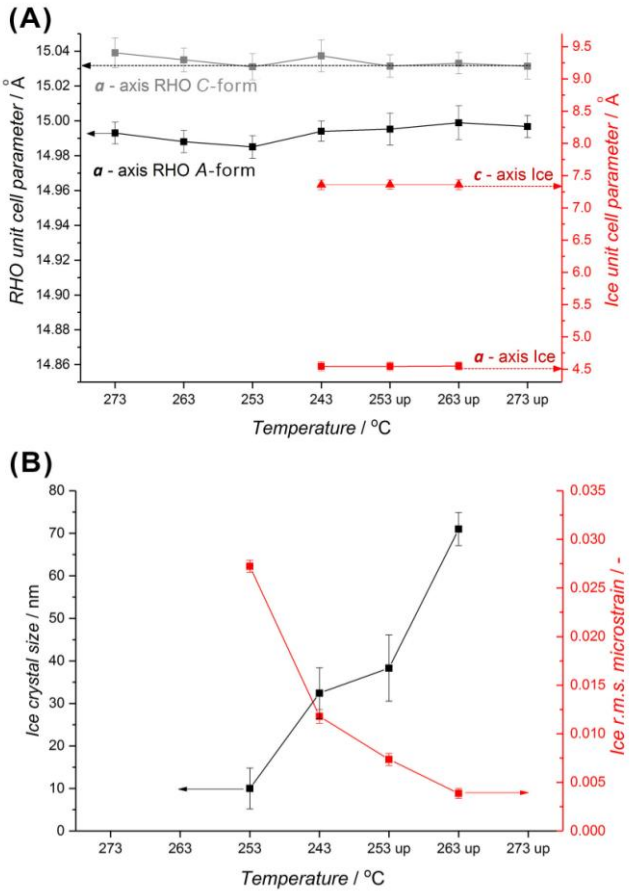

Figure 5. Evolution of (*a*) unit cell parameters for centric (*C*-form, *Im*-3*m*) and acentric (*A*-form, *I*-43*m*)

phases of RHO zeolite and hexagonally packed ice ($P6_3cm$); (*b*) crystal sizes (black squares) and microstrain parameters (red squares) for hexagonally packed ice ($P6_3cm$) over temperature range from 273 K to 243 K and up again to 273 K. The error bars are shown for each parameter at all studied temperatures.

In a second set of temperature programmed experiments, the methane gas at the pressure of 3 MPa was supplied to the hydrated RHO zeolite and PXRD patterns were acquired from 273 K to 233 K and back to 273 K. Comparison of the experimental data (Figure 6.a) with the theoretically expected patterns for both configurations of RHO zeolite shows the coexistence of both centric (*Im*-3*m*) and acentric (*I*-43*m*) phases of RHO framework in the hydrated zeolite at 3 MPa of methane atmosphere. The crystallization of hexagonally packed ice structure is started at 243 K as well as in the previous set of experiments performed at normal pressure and without methane. The methane hydrate formation could not be observed while cooling and it was only initiated while warming at 253 K and continued growing until the temperature reaches 273 K (Figure 6.b), as was confirmed by typical diffraction lines originated from cubic methane clathrate structure (*sI*) (*Pm*-3*n*) [44]. Moreover, methane clathrate structure of type I (*sI*) was expected based on the size of methane molecules, and the selected pressure and temperature conditions. Interestingly, the hydrate formation is completely followed by ice melting process. The maximum of crystallinity for methane clathrate falls in the temperature range where the ice completely becomes amorphous. The most noticeable fact is the absence of methane clathrate formation at the decreasing temperature section – It is observed at similar temperature levels in the increasing range, when water was present as crystalline ice. Some formation theories pointed out the importance of clathrate residual structure to form new ones. Recent study of methane clathrate formation on ZIF-8 throughout several consecutive cycles showed a surface memory effect/preorganization in these materials promoting gas hydrate formation in the following repetitions, suggesting that residual crystalline ice structures have an important role in the methane hydrate formation process [17].

The quantitative analyses of synchrotron X-ray diffraction patterns acquired for hydrated RHO zeolite under constant methane pressure of 3 MPa and for temperatures from 273 K down to 233 K and up again to 278 K (Figure 6.c) show a higher contribution of C-RHO phase on the amount of crystalline ice formed. Notably, the weight fraction of acentric RHO form and crystalline I_h ice yielded during the process is twice as much as in experiments performed at normal pressure and without methane. The contents of acentric RHO phase and ice evolve dependently along the temperature range from 263 K to 233 K and up again to 278 K. This observed trend suggests the participation of the hydrated *C*-RHO phase on the ice crystallization process as have been discussed previously. The amorphization of the crystalline ice structure is followed by formation of methane hydrate, which begins at 253 K and reaches the maximum of crystallinity at 273 K with a weight fraction contribution of 19%. These results confirm that the methane clathrate formation occurs when the water is present as amorphous phase.

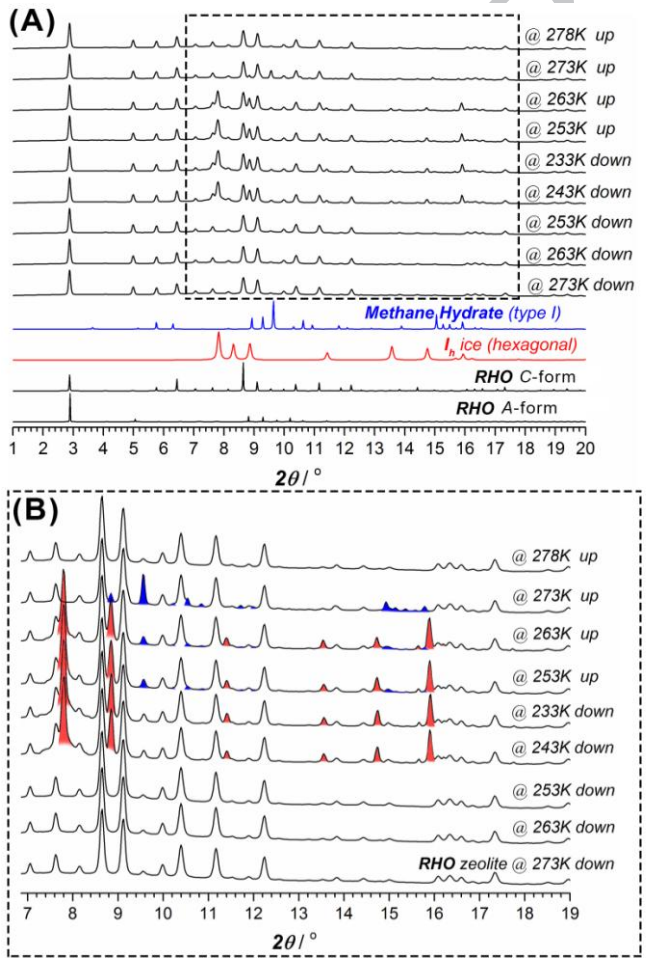

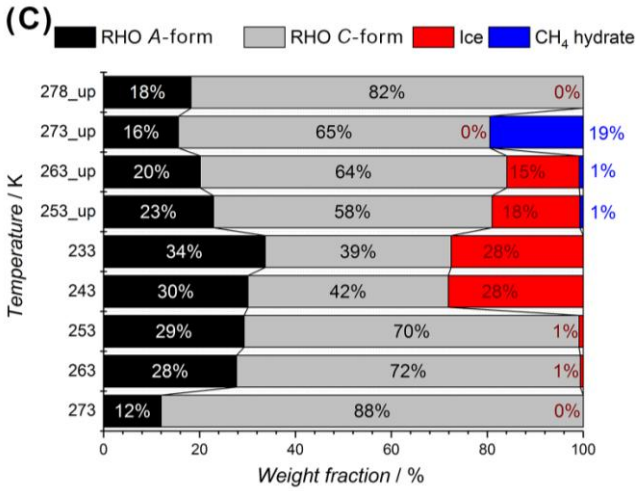

Figure 6. (*a*) Series of the powder X-ray diffraction patterns of hydrated RHO sample acquired at methane pressure of 3 MPa and different temperatures, down from 273 K to 233 K and up again to 278 K, compared to the expected patterns for centric (*C*-form, *Im*-3*m*) and acentric (*A*-form, *I*-43*m*) phases of RHO zeolite; hexagonally packed ice structure (I_h) and cubic methane hydrate (*Pm*-3*n*). (*b*) Inset shows the enlarged 2θ region where typical diffraction lines originated from the hexagonal ice structure (I_h) and methane hydrate (*sI*) are highlighted in red and blue, respectively. (*c*) The evolution of weight fraction for centric, acentric phases of RHO zeolite, crystalline ice and methane hydrate structure in the mixture over temperature range from 273 K to 233 K and up again to 278 K and constant pressure of methane (3 MPa).

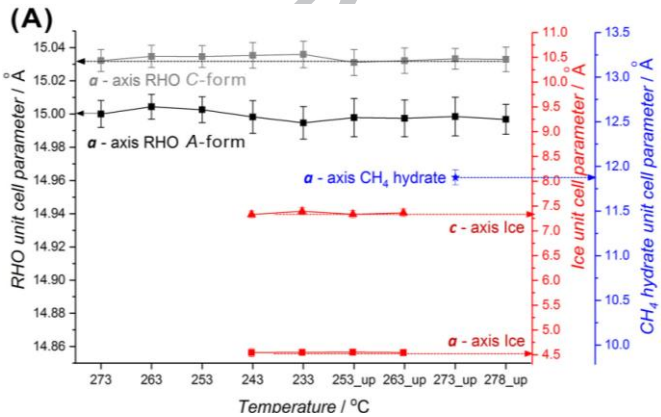

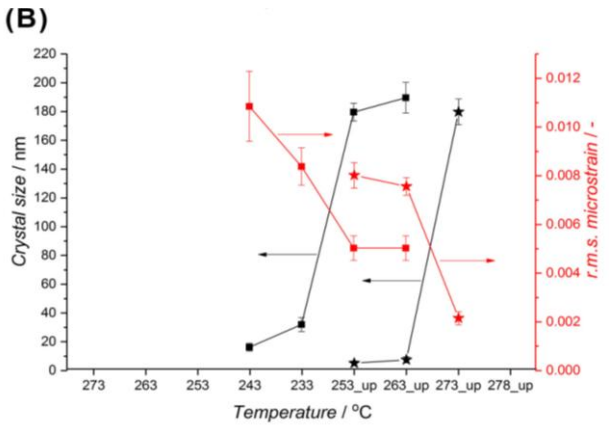

Figure 7. Evolution of (*a*) unit cell parameters for centric (*C*-form, *Im*-3*m*) and acentric (*A*-form, *I*-43*m*) phases of RHO zeolite, hexagonally packed ice ($P6_3cm$) and cubic methane hydrate (*Pm*-3*n*); (*b*) crystal sizes (black lines) and microstrain parameters (red lines) for hexagonally packed ice ($P6_3cm$, squares) and cubic methane hydrate (*Pm*-3*n*, stars) over temperature range from 273 K to 233 K and up again to 278 K and constant pressure of methane (3 MPa). The error bars are shown for each parameter at all studied temperatures.

It worth to note that in the set of experiments with methane, the magnitude of phase transitions and the relative content of centric and acentric RHO phases are larger than those without methane. This behaviour originates from the competitive replacement of water molecules located in the zeolite pores by methane molecules. Water mobility is also encouraged by the re-heating the zeolite, promoting that gas displacement. Adsorption isotherms already indicated this effect of methane saturation before hydrate formation. As shown on Figure 7.a, the unit cell parameters development for both RHO phases, ice and methane clathrate structures do not change considerably over the whole temperature range studied. These results further confirm the absence of large deformations in the zeolite structure related to the encapsulation of crystalline ice or methane hydrate into RHO framework. Additionally, crystal size and macrostrain parameters show the expected evolution trend corresponding to growing crystals of ice and methane hydrate (Figure 7.b).

In order to analyse further the kinetics of methane hydrate formation at two remarkable temperatures, the isothermal evolution of hydrates along the time at 273 K and 278 K are presented in Figure 8.a-b. After going down from 298 K to 243 K, and up again, temperature is set at 273 K (on 3 MPa methane). At that point (Figure 8.a), crystalline ice melts to provide the liquid water needed in

hydrate formation. Ice reflections (*i*) disappear in favour of the hydrate ones (*c*). At 278 K (Figure 8.b), hydrate structure decomposes. Reflections related to hydrates vanish, thus only the zeolite-related pattern remains at the end of the reversible formation process. PXRD patterns confirmed the presence of ice at low temperature in RHO zeolite; ice was crystalline from 243 K, and remained in this configuration when temperature increased. The presence of high-pressure methane in the same sample, above 253 K, promoted the appearance of hydrates.

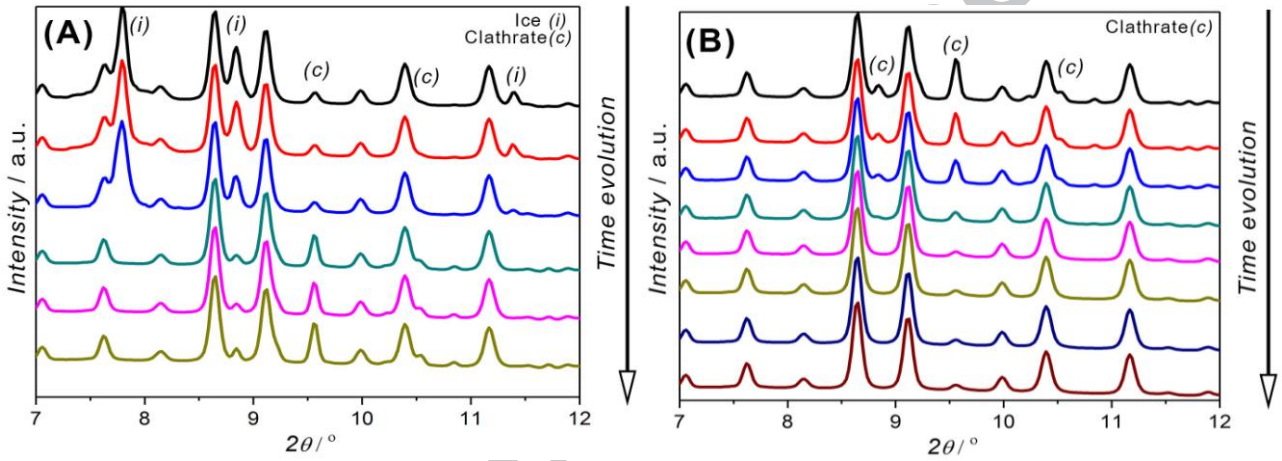

Figure 8. Evolution with time of PXRD patterns for wet RHO zeolite at 273 K (*a*) and at 278 K (*b*) under methane pressure of 3 MPa. Reflections corresponding to ice and methane hydrate are marked as (*i*) and (*c*).

Based on the cell parameters from the PXRD analysis, and the framework morphology, it is concluded that clathrates are formed outside the zeolite and not in the pores. Since initially methane and water are also present inside the zeolite, and become consumed, these species feed initially the first clathrate layer, in addition to supply from the outside environment in later stages.

For further growth of the clathrate, both nutrients (water and methane) need to reach the nucleation surface of the zeolite, thus the growing is promoted from inside of the existing clathratic crown. Methane needs to diffuse through the already formed hydrate shell to the zeolitic core. This diffusion through clathrates is fast [45], so is not a rate determining process.

4. Conclusions

This study focuses on in-depth study of the methane clathrate formation over pre-humidified RHO zeolite. Adsorption isotherms and *in-situ* synchrotron X-ray diffraction measurements evidenced the formation of methane hydrate structure. Under methane pressure of 3 MPa, the clathrate crystallization starts at 253 K and reaches its maximum of crystallinity at 273 K. Detailed X-ray diffraction analysis including quantification and evaluation of unit cell parameters suggested that RHO zeolite grains could act as nucleation sites for methane clathrate growth. Furthermore, the crystalline ice promotes hydrate formation and acts as nutrient for the further crystal growth. Both centric and acentric phases of RHO zeolite coexist as individual crystallite domains within the same zeolite grain; and the centric phase of RHO zeolite transforms into dehydrated acentric RHO form as an effect of the ice crystals formation and zeolite drying. The methane hydrate formation process over pre-humidified RHO zeolite can be divided into three steps: *i*) saturation of RHO zeolite with methane and draining of resided in the pores water molecules towards external surface of the zeolite grain; *ii*) in turn, the zeolite grain surface enriched with amorphous ice provides both the nucleation sites and nutrients for the formation of methane hydrates crown; *iii*) growing clathrate shell consumes the methane molecules supplied through the amorphous ice phase by the pressurised atmosphere. Cell volume and available water molecules determine the extent of hydrates formation.

Acknowledgements

ITQ belongs to University of Valencia (UPV) and to the Superior Council of Scientific Investigations (CSIC - Consejo Superior de Investigaciones Científicas), also located in the UPV Campus. Financial support from Generalitat Valenciana (project PROMETEOII/2014/004) and MINECO (Project MAT2013-45008-P) is gratefully acknowledged. EVRF also thanks MINECO for his Ramon y Cajal fellow RYC-2012-11427 and the following projects: MAT2016-81732-ERC and MAT2017-86992-R. Alba synchrotron is also acknowledged for the experiment 2016021678.

References

[1] P. Longone, A. Martín, A.J. Ramirez-Pastor, Stability and cell distortion of sI clathrate hydrates of methane and carbon dioxide: A 2D lattice-gas model study, Fluid Phase Equilibria, 402 (2015) 30-37.

[2] M.H.R. Stackelberg M. v., On the Structure of Gas Hydrates, Naturwiss, 38 (1951) 456.

[3] W.F. Claussen, Suggested Structures of Water in Inert Gas Hydrates, J. Chem Phys 19 (1951) 259-632

[4] P. Villard, On the Carbonic Hydrate and the Composition of Gas Hydrates, Acad. Sci. Paris, Comptes rendus, 119 (1988) 368-371.

[5] H.M. Powell, The structure of molecular compounds. Part VII. Compounds formed by the inert gases, J. Chem. Soc., (1950) 298-300.

[6] P.E. Brumby, D. Yuhara, D.T. Wu, A.K. Sum, K. Yasuoka, Cage occupancy of methane hydrates from Gibbs ensemble Monte Carlo simulations, Fluid Phase Equilibria, 413 (2016) 242-248.

[7] B. Fang, F. Ning, P. Cao, L. Peng, J. Wu, Z. Zhang, T.J.H. Vlugt, S. Kjelstrup, Modeling Thermodynamic Properties of Propane or Tetrahydrofuran Mixed with Carbon Dioxide or Methane in Structure-II Clathrate Hydrates, The Journal of Physical Chemistry C, 121 (2017) 23911-23925.

[8] H. Pahlavanzadeh, M. Khanlarkhani, A.H. Mohammadi, Clathrate hydrate formation in (methane, carbon dioxide or nitrogen + tetrahydropyran or furan + water) system: Thermodynamic and kinetic study, The Journal of Chemical Thermodynamics, 92 (2016) 168-174.

[9] H. Lee, J.-w. Lee, D.Y. Kim, J. Park, Y.-T. Seo, H. Zeng, I.L. Moudrakovski, C.I. Ratcliffe, J.A. Ripmeester, Tuning clathrate hydrates for hydrogen storage, Nature, 434 (2005) 743-746.

[10] J.A. Ripmeester, S. Alavi, Some current challenges in clathrate hydrate science: Nucleation, decomposition and the memory effect, Current Opinion in Solid State and Materials Science, 20 (2016) 344-351.

[11] M.R. Walsh, J.D. Rainey, P.G. Lafond, D.-H. Park, G.T. Beckham, M.D. Jones, K.-H. Lee, C.A. Koh, E.D. Sloan, D.T. Wu, A.K. Sum, The cages, dynamics, and structuring of incipient methane clathrate hydrates, Physical Chemistry Chemical Physics, 13 (2011) 19951-19959.

[12] T.A. Strobel, K.C. Hester, C.A. Koh, A.K. Sum, E.D. Sloan, Properties of the clathrates of hydrogen and developments in their applicability for hydrogen storage, Chemical Physics Letters, 478 (2009) 97-109.

[13] G.J. MacDonald, Role of methane clathrates in past and future climates, Climatic Change, 16 (1990) 247-281.

[14] M.E. Casco, J. Silvestre-Albero, A.J. Ramírez-Cuesta, F. Rey, J.L. Jordá, A. Bansode, A. Urakawa, I. Peral, M. Martínez-Escandell, K. Kaneko, F. Rodríguez-Reinoso, Methane hydrate formation in confined nanospace can surpass nature, Nat Commun, 6 (2015).

[15] A. Perrin, A. Celzard, J.F. Marêché, G. Furdin, Improved methane storage capacities by sorption on wet active carbons, Carbon, 42 (2004) 1249-1256.

[16] B. Lars, C.M. Elizabeth, S.A. Joaquin, Methane Hydrate in Confined Spaces: An Alternative Storage System, ChemPhysChem, 0.

[17] M.E. Casco, F. Rey, J.L. Jorda, S. Rudic, F. Fauth, M. Martinez-Escandell, F. Rodriguez-Reinoso, E.V. Ramos-Fernandez, J. Silvestre-Albero, Paving the way for methane hydrate formation on metal-organic frameworks (MOFs), Chemical Science, 7 (2016) 3658-3666.

[18] X. Zang, J. Du, D. Liang, S. Fan, C. Tang, Influence of A-type Zeolite on Methane Hydrate Formation, Chinese Journal of Chemical Engineering, 17 (2009) 854-859.

[19] H. Noguchi, A. Kondoh, Y. Hattori, H. Kanoh, H. Kajiro, K. Kaneko, Clathrate-Formation Mediated Adsorption of Methane on Cu-Complex Crystals, The Journal of Physical Chemistry B, 109 (2005) 13851-13853.

[20] P. Warrier, M.N. Khan, V. Srivastava, C.M. Maupin, C.A. Koh, Overview: Nucleation of clathrate hydrates, The Journal of Chemical Physics, 145 (2016) 211705.

[21] R.W. Hawtin, D. Quigley, P.M. Rodger, Gas hydrate nucleation and cage formation at a water/methane interface, Physical Chemistry Chemical Physics, 10 (2008) 4853-4864.

[22] M. Lauricella, G. Ciccotti, N.J. English, B. Peters, S. Meloni, Mechanisms and Nucleation Rate of Methane Hydrate by Dynamical Nonequilibrium Molecular Dynamics, The Journal of Physical Chemistry C, 121 (2017) 24223-24234.

[23] P.W. Wilson, A.D.J. Haymet, Hydrate formation and re-formation in nucleating THF/water mixtures show no evidence to support a “memory” effect, Chemical Engineering Journal, 161 (2010) 146-150.

[24] J. E. Dendy Sloan, Clathrate Hydrates of Natural Gases, Second Edition, Revised and Expanded, 2nd ed., 1998.

[25] M. Lauricella, S. Meloni, N.J. English, B. Peters, G. Ciccotti, Methane Clathrate Hydrate Nucleation Mechanism by Advanced Molecular Simulations, The Journal of Physical Chemistry C, 118 (2014) 22847-22857.

[26] L.C. Jacobson, W. Hujo, V. Molinero, Amorphous Precursors in the Nucleation of Clathrate Hydrates, Journal of the American Chemical Society, 132 (2010) 11806-11811.

[27] N.J. English, J.M.D. MacElroy, Perspectives on molecular simulation of clathrate hydrates: Progress, prospects and challenges, Chemical Engineering Science, 121 (2015) 133-156.

[28] K. Nam‐Jin, P. Sung‐Seek, S. Sang‐Woong, H. Jun‐Ho, C. Wongee, An experimental investigation into the effects of zeolites on the formation of methane hydrates, International Journal of Energy Research, 39 (2015) 26-32.

[29] W.S. Wise, MINERALS | Zeolites, in: Reference Module in Earth Systems and Environmental Sciences, Elsevier, 2013.

[30] C. Baerlocher, McCusker, L.B., Database of Zeolite Structures, in.

[31] D.W. Breck, Zeolite Molecular Sieves, 1974.

[32] M. Pera-Titus, M. Palomino, S. Valencia, F. Rey, Thermodynamic analysis of framework deformation in Na,Cs-RHO zeolite upon CO2 adsorption, Physical Chemistry Chemical Physics, 16 (2014) 24391-24400.

[33] C. Baerlocher, L.B. McCusker, D.H. Olson, RHO - Im3¯m, in: C. Baerlocher, L.B.M.H. Olson (Eds.) Atlas of Zeolite Framework Types (Sixth Edition), Elsevier Science B.V., Amsterdam, 2007, pp. 266-267.

[34] D.R. Corbin, L. Abrams, G.A. Jones, M.M. Eddy, W.T.A. Harrison, G.D. Stucky, D.E. Cox, Flexibility of the zeolite RHO framework: in situ x-ray and neutron powder structural characterization of divalent cation-exchanged zeolite RHO, Journal of the American Chemical Society, 112 (1990) 4821-4830.

[35] M.M.J. Treacy, J.B. Higgins, RHO - Rho, Hydrated, in: M.M.J. Treacy, J.B. Higgins (Eds.) Collection of Simulated XRD Powder Patterns for Zeolites (fifth), Elsevier Science B.V., Amsterdam, 2007, pp. 348-349.

[36] M. Palomino, A. Corma, J.L. Jorda, F. Rey, S. Valencia, Zeolite Rho: a highly selective adsorbent for CO2/CH4 separation induced by a structural phase modification, Chemical Communications, 48 (2012) 215-217.

[37] ITQ (Instituto de Tecnología Química - Chemical Technology Institute) in.

[38] L. Lutterotti, Total Pattern Fitting for the Combined Size-Strain-Stress-Texture Determination in Thin Film Diffraction, 2010.

[39] D.R. Corbin, L. Abrams, G.A. Jones, R.L. Harlow, P.J. Dunn, Flexibility of the zeolite RHO framework: Effect of dehydration on the crystal structure of the beryllophosphate mineral, pahasapaite, Zeolites, 11 (1991) 364-367.

[40] J.M. Schicks, M. Luzi-Helbing, Kinetic and Thermodynamic Aspects of Clathrate Hydrate Nucleation and Growth, Journal of Chemical & Engineering Data, 60 (2015) 269-277.

[41] T. Yagasaki, M. Matsumoto, H. Tanaka, Mechanism of Slow Crystal Growth of Tetrahydrofuran Clathrate Hydrate, The Journal of Physical Chemistry C, 120 (2016) 3305-3313.

[42] J. Miyawaki, T. Kanda, T. Suzuki, T. Okui, Y. Maeda, K. Kaneko, Macroscopic Evidence of Enhanced Formation of Methane Nanohydrates in Hydrophobic Nanospaces, The Journal of Physical Chemistry B, 102 (1998) 2187-2192.

[43] A Theory of Water and Ionic Solution, with Particular Reference to Hydrogen and Hydroxyl Ions, The Journal of Chemical Physics, 1 (1933) 515-548.

[44] M.T. Kirchner, R. Boese, W.E. Billups, L.R. Norman, Gas Hydrate Single-Crystal Structure Analyses, Journal of the American Chemical Society, 126 (2004) 9407-9412.

[45] U. Ranieri, M.M. Koza, W.F. Kuhs, S. Klotz, A. Falenty, P. Gillet, L.E. Bove, Fast methane diffusion at the interface of two clathrate structures, Nature Communications, 8 (2017) 1076.

Highlights:

- *Hydrated RHO zeolite promotes methane hydrates formation at mild pressure conditions.*
- *RHO zeolite provides nucleation sites to initiate this process.*
- *Methane hydrates grow outside the RHO zeolite.*
- *This publication provides the highest methane adsorbed volume per gram of microporous material.*

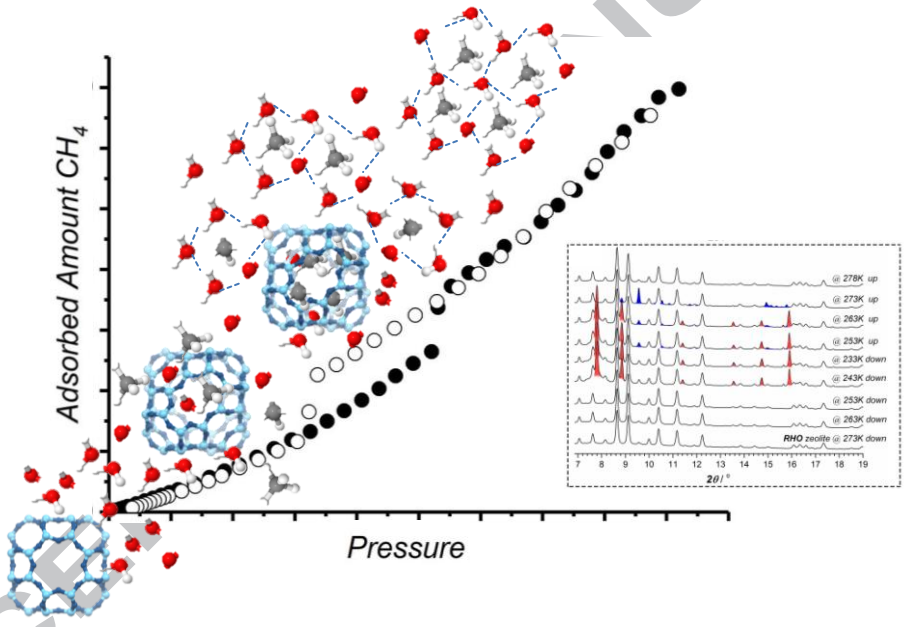

Appendix 1

Methane Hydrates: Nucleation in Microporous Materials

Eduardo Andres-Garcia[a*], Alla Dikhtiarenko[b], Francois Fauth[c], Joaquin Silvestre-Albero[d], Enrique V. Ramos-Fernández[d], Jorge Gascon[b], Avelino Corma[e] and Freek Kapteijn[a*]

Figures A.1 and A.2 complete RHO characterization with SEM images and H_2O isotherm at 298 K.
Figures A.3 and A.4 display adsorption/desorption isotherms for CO_2 and CH_4 at 273 K, 298 K, 313 K and 323 K.
Figure A.5. 2D plot of synchrotron X-ray diffraction patterns acquired for pre-humidified RHO zeolite sample without methane at variable temperatures
Figure A.6. 2D plot of synchrotron X-ray diffraction patterns acquired for pre-humidified RHO zeolite sample with methane pressure of 3 MPa at variable temperatures
Table A.1. Summary of crystal data, quantitative analysis and refinement parameters for pre-humidified RHO zeolite sample without methane at variable temperatures
Table A.2. Summary of crystal data, quantitative analysis and refinement parameters for pre-humidified RHO zeolite sample with methane pressure of 3 MPa at variable temperatures
Figure A.7. CH4 adsorption/desorption isotherm measured at 278 K over 5% THF miliQ water (no RHO zeolite sample) at equilibration time of 60,000 seconds. Solid symbols correspond to the adsorption curve and open ones for desorption.

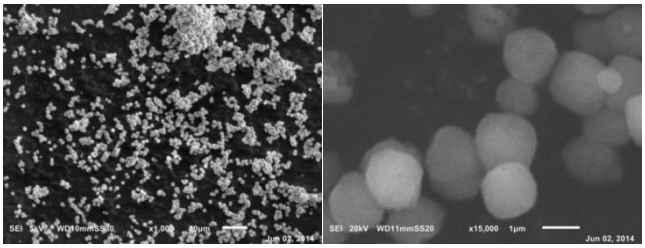

Figure A.1. RHO particles in SEM (a) V:5kW; SS:30; MAG:1000 (b) V:20kW; SS:20; MAG:15000.

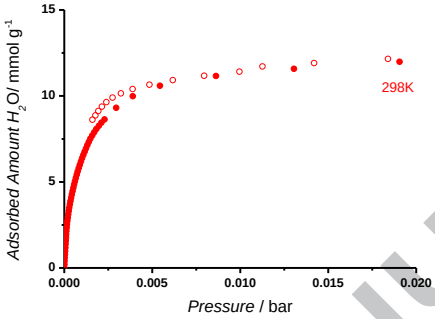

Figure A.2. Adsorption/desorption isotherm for H_2O at 298 K, in powder RHO zeolite. (Solid symbols for adsorption and open ones for desorption)

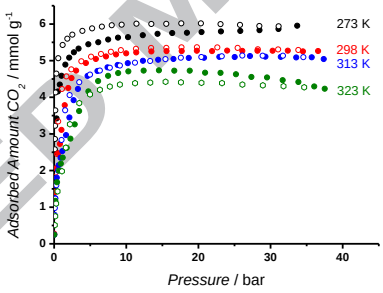

Figure A.3. Adsorption/desorption isotherms for CO_2 at 273 K (*black*), 298 K (*red*), 313 K (*blue*) and 323 K (*green*), in powder RHO zeolite. (solid symbols for adsorption and open ones for desorption)

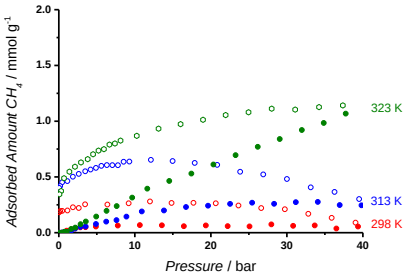

Figure A.4. Adsorption/desorption uptakes for CH_4 at 298 K (*red*), 313 K (*blue*) and 323 K (*green*), in powder RHO zeolite. (Solid symbols for adsorption and open ones for desorption)

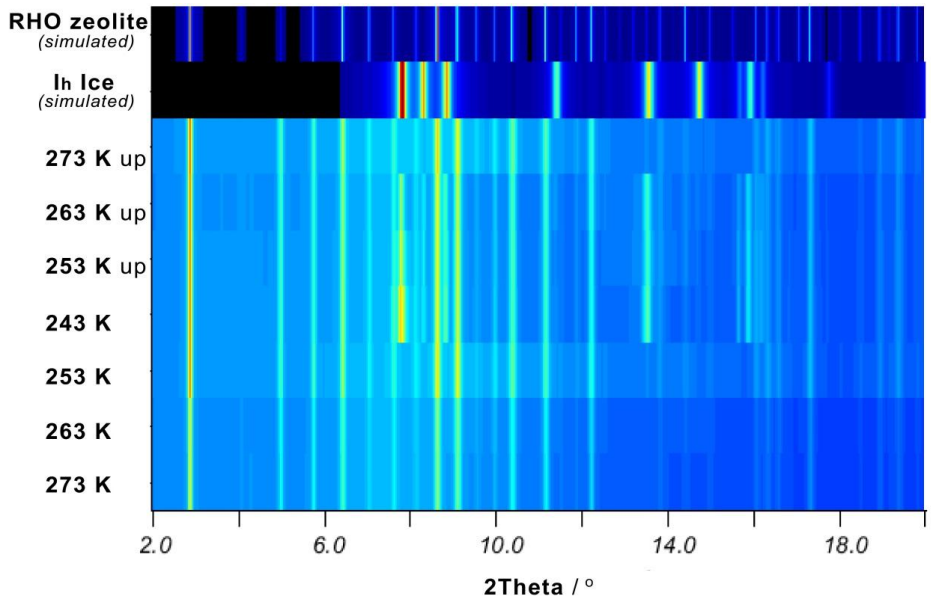

Figure A.5. 2D plot of synchrotron X-ray diffraction patterns acquired for pre-humidified RHO zeolite sample without methane at variable temperatures from 273 K to 243 K and up again to 273 K, and compared to the expected diffractograms for RHO zeolite and hexagonally packed ice I_h structure.

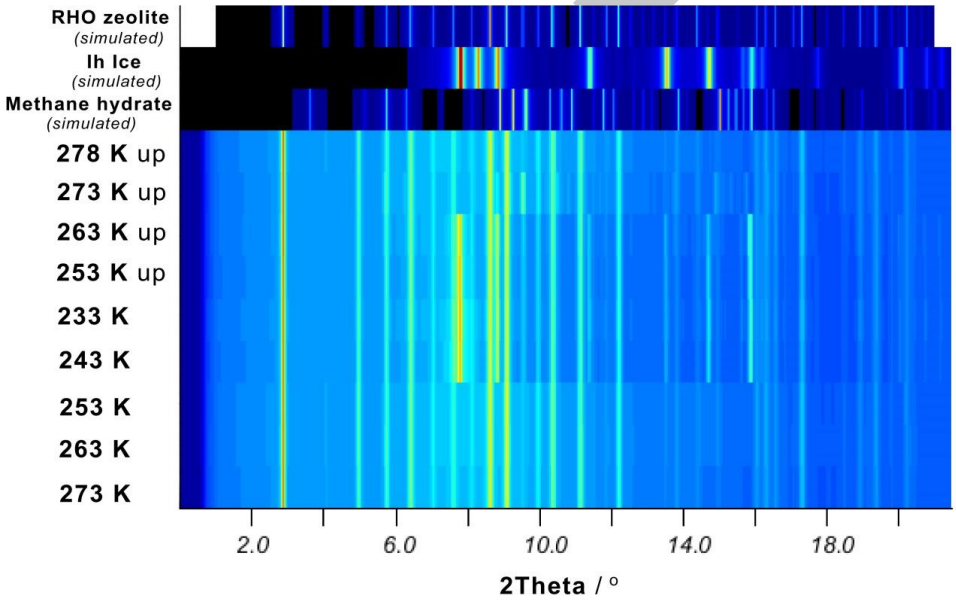

Figure A.6. 2D plot of synchrotron X-ray diffraction patterns acquired for pre-humidified RHO zeolite sample with methane pressure of 3 MPa at variable temperatures from 273 K to 233 K and up again to 278 K, and compared to the expected diffractograms for RHO zeolite, hexagonally packed ice I_h and methane clathrate *s*I structures.

Table A.1. Summary of crystal data, quantitative analysis and refinement parameters for pre-humidified RHO zeolite sample without methane at variable temperatures: cooling down from 273 K to 243 K and heating up again to 273 K.

Temperature / K	Parameter	RHO A-form	RHO dehydrated	Ice
273	*a* / Å	15.035 ± 0.007	14.988 ± 0.006	–
	c / Å	15.035 ± 0.007	14.988 ± 0.006	
	Weight fraction / %	88 ± 3	12 ± 1	
	R_w, R_{wnb} / %	3.94, 4.95		
	R_B / %	2.64		
263	*a* / Å	15.031 ± 0.007	14.988 ± 0.006	–
	c / Å	15.031 ± 0.007	14.988 ± 0.006	
	Weight fraction / %	88 ± 5	12 ± 3	
	R_w, R_{wnb} / %	3.98, 5.11		
	R_B / %	2.66		
	a / Å	15.031 ± 0.007	14.985 ± 0.006	

	c / Å	15.031 ± 0.007		14.985 ± 0.006	
253	Weight fraction / %	85 ± 3		14 ± 1	0.8 ± 0.04
	R_w, R_{wnb} / %		6.45, 8.68		
	R_B / %		4.01		
	a / Å	15.037 ± 0.009		14.994 ± 0.006	4.54 ± 0.07
	c / Å	15.037 ± 0.009		14.994 ± 0.006	7.36 ± 0.07
243	Weight fraction / %	61 ± 4		18 ± 1	21 ± 2
	R_w, R_{wnb} / %		13.03, 15.06		
	R_B / %		9.47		
	a / Å	15.031 ± 0.006		14.995 ± 0.009	4.54 ± 0.06
	c / Å	15.031 ± 0.006		14.995 ± 0.009	7.36 ± 0.07
253 up	Weight fraction / %	66 ± 3		16 ± 1	18 ± 1
	R_w, R_{wnb} / %		12.48, 14.71		
	R_B / %		8.98		
	a / Å	15.033 ± 0.006		14.998 ± 0.009	4.54 ± 0.06
	c / Å	15.033 ± 0.006		14.998 ± 0.009	7.36 ± 0.08
263 up	Weight fraction / %	68 ± 2		14 ± 1	17.2 ± 0.6
	R_w, R_{wnb} / %		11.83, 13.72		
	R_B / %		8.40		
	a / Å	15.031 ± 0.007		14.997 ± 0.006	
	c / Å	15.031 ± 0.007		14.997 ± 0.006	
273 up	Weight fraction / %	86 ± 3		14 ± 1	–
	R_w, R_{wnb} / %		5.42, 6.17		
	R_B / %		3.85		

Table A.2. Summary of crystal data, quantitative analysis and refinement parameters for pre-humidified RHO zeolite sample with methane pressure of 3 MPa at variable temperatures from 273 K to 233 K and up again to 278 K.

Temperature / K	Parameter	RHO hydrated	RHO dehydrated	Ice	CH_4 Hydrate
	a / Å	15.032 ± 0.006	15.000 ± 0.008		
	c / Å	15.032 ± 0.006	15.000 ± 0.008		
273	Weight fraction / %	88 ± 6	12 ± 4	–	–
	R_w, R_{wnb} / %		5.49, 6.99		
	R_B / %		3.79		
	a / Å	15.035 ± 0.007	15.004 ± 0.007		
	c / Å	15.035 ± 0.007	15.004 ± 0.007		
263	Weight fraction / %	72 ± 6	28 ± 8	–	–
	R_w, R_{wnb} / %		5.56, 7.22		
	R_B / %		3.83		
	a / Å	15.035 ± 0.007	15.003 ± 0.008		
	c / Å	15.035 ± 0.007	15.003 ± 0.008		
253	Weight fraction / %	70 ± 5	29 ± 5	~ 0.9	–
	R_w, R_{wnb} / %		5.80, 7.52		
	R_B / %		3.99		
	a / Å	15.035 ± 0.007	14.998 ± 0.009	4.54 ± 0.08	
	c / Å	15.035 ± 0.007	14.998 ± 0.009	7.33 ± 0.07	
243	Weight fraction / %	42 ± 3	30 ± 2	28 ± 3	–
	R_w, R_{wnb} / %		11.51, 15.21		
	R_B / %		7.78		
	a / Å	15.035 ± 0.008	14.995 ± 0.009	4.55 ± 0.06	
	c / Å	15.035 ± 0.008	14.995 ± 0.009	7.39 ± 0.07	
233	Weight fraction / %	39 ± 4	34 ± 6	28 ± 2	–
	R_w, R_{wnb} / %		11.59, 15.31		
	R_B / %		7.80		
	a / Å	15.031 ± 0.008	14.997 ± 0.011	4.55 ± 0.06	
	c / Å	15.031 ± 0.008	14.997 ± 0.011	7.33 ± 0.08	
253 up	Weight fraction / %	58 ± 4	23 ± 3	18 ± 1	0.75 ± 0.1
	R_w, R_{wnb} / %		11.53, 15.21		
	R_B / %		7.80		
	a / Å	15.032 ± 0.007	14.997 ± 0.011	4.54 ± 0.06	
	c / Å	15.032 ± 0.007	14.997 ± 0.011	7.36 ± 0.07	

263 up	Weight fraction / %	64 ± 5	20 ± 4	15 ± 3	0.82 ± 0.1
	R_w, R_{wnb} / %	11.27, 15.38			
	R_B / %	7.49			
	a / Å	15.033 ± 0.006	14.998 ± 0.011		11.87 ± 0.08
	c / Å	15.033 ± 0.006	14.998 ± 0.011		11.87 ± 0.08
273 up	Weight fraction / %	65 ± 2	16 ± 1	~ 0.7	19 ± 1
	R_w, R_{wnb} / %	7.07, 7.59			
	R_B / %	5.65			
	a / Å	15.033 ± 0.007	14.997 ± 0.009		
	c / Å	15.033 ± 0.007	14.997 ± 0.009		
278 up	Weight fraction / %	82 ± 2	18 ± 1	–	–
	R_w, R_{wnb} / %	5.73, 6.74			
	R_B / %	4.43			

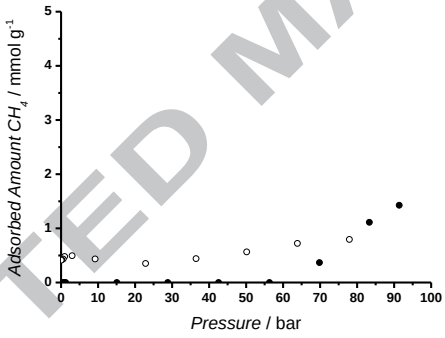

Figure A.7. CH_4 adsorption/desorption isotherm measured at 278 K over 5% THF miliQ water (no RHO zeolite sample) at equilibration time of 60,000 s. Solid symbols correspond to the adsorption branch and open ones for desorption.

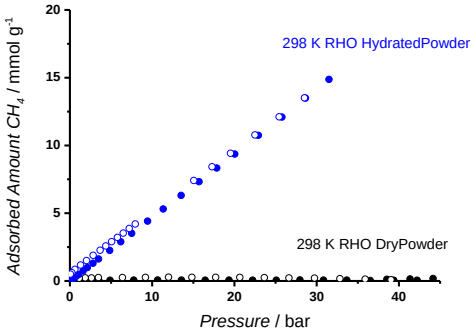

Figure A.8. CH_4 adsorption/desorption isotherms measured at 298 K for dry and hydrated (miliQ water) RHO zeolite powder, at equilibration time of 600 s. Solid symbols correspond to the adsorption branch and open ones for desorption.